Research Article

Large-inductance superconducting microstrip photon detector enabling 10 photon-number resolution
==

Ling-Dong Kong,[a,b,*,†] Tian-Zhu Zhang,[a,b,†] Xiao-Yu Liu,[a,b] Hao Li,[a,b] Zhen Wang,[a,b] Xiao-Ming Xie,[a,b] and Li-Xing You ◉[a,b,c,*]

[a]Chinese Academy of Sciences (CAS), Shanghai Institute of Microsystem and Information Technology, National Key Laboratory of Materials for Integrated Circuits, Shanghai, China
[b]CAS Center for Excellence in Superconducting Electronics, Shanghai, China
[c]University of Chinese Academy of Sciences, Center of Materials Science and Optoelectronics Engineering, Beijing, China

Abstract. Efficient and precise photon-number-resolving detectors are essential for optical quantum information science. Despite this, very few detectors have been able to distinguish photon numbers with both high fidelity and a large dynamic range, all while maintaining high speed and high timing precision. Superconducting nanostrip-based detectors excel at counting single photons efficiently and rapidly, but face challenges in balancing dynamic range and fidelity. Here, we have pioneered the demonstration of 10 true photon-number resolution using a superconducting microstrip detector, with readout fidelity reaching an impressive 98% and 90% for 4-photon and 6-photon events, respectively. Furthermore, our proposed dual-channel timing setup drastically reduces the amount of data acquisition by 3 orders of magnitude, allowing for real-time photon-number readout. We then demonstrate the utility of our scheme by implementing a quantum random-number generator based on sampling the parity of a coherent state, which guarantees inherent unbiasedness, robustness against experimental imperfections and environmental noise, as well as invulnerability to eavesdropping. Our solution boasts high fidelity, a large dynamic range, and real-time characterization for photon-number resolution and simplicity with respect to device structure, fabrication, and readout, which may provide a promising avenue towards optical quantum information science.

Keywords: superconducting microstrips; single-photon detector; photon-number resolution; quantum random number.

1 Introduction

Single photons acting as qubits have emerged as a prominent approach to quantum information technology.[1–3] The ability to accurately discriminate the photon number cannot be overstated in various quantum systems, including linear optical quantum computation,[4,5] preparation[6] and characterization[7,8] of quantum light sources, quantum random number generation,[9] as well as quantum-enhanced communication[10] and detection[11] in general. In these schemes, information on quantum states is primarily monitored with photon-number-resolving detectors (PNRDs), whose resolving fidelity and dynamic range greatly affect operating accuracy. The PNR fidelity is defined as the probability of accurately recording the number of incident photons.[12] It is simultaneously determined by detection efficiency, readout fidelity (the separating degree of neighboring photon numbers in readout features), and splitting fidelity, particularly in the case of spatial-multiplexing arrays (the probability of all photons simultaneously activating different pixels). Extensive efforts have been dedicated to the advancement of

---

*Address all correspondence to Ling-Dong Kong, ldkong@mail.sim.ac.cn; Li-Xing You, lxyou@mail.sim.ac.cn

†These authors contributed equally to this work.

PNRDs,[13,14] yet their dynamic range and fidelity remain constrained by either significant readout overlap[15–17] or low detection efficiency.[18] Superconducting transition edge sensors (TESs), as the most successful PNRDs so far, can achieve high-fidelity PNR over 30 photons.[9] However, their operation at ultralow temperatures (∼100 mK) poses a challenge, and the trade-off between PNR capability and recovery time restricts their counting rate,[14] which is also undesirable for quantum information applications.

Superconducting nanostrip single-photon detectors (SNSPDs)[19] are a cutting-edge single-photon detection technology, renowned for near-unity detection efficiency,[20–22] negligible dark counts,[23,24] gigahertz-level counting rate,[25,26] and timing jitter at the picosecond scale.[27] These exceptional attributes have catapulted them to significant applications within the field of quantum information technology.[28] However, unlike TESs, SNSPDs possess an inherently weak PNR ability[29] due to the highly nonlinear signal amplification through hotspot resistance following a single photon detection.[30] Most existing solutions are primarily aimed at implementing spatial-multiplexing arrays to distribute the optical wave packet amongst multiple pixels.[26,31,32] In these quasi-PNR detectors, to achieve high fidelity, the pixels must significantly outnumber the incident photons to minimize the likelihood of multiple photons striking the same pixel. Even with perfect efficiency and readout distinguishability, a 100-pixel detector can only achieve fidelity of less than 90% at over-5-photon detection.[33] On the other hand, the presence of a localized hotspot resistor controlled by electrothermal feedback suggests that an SNSPD with an adequately long superconducting nanostrip is equivalent to a cascade of thousands of elements and n photons simultaneously activating different elements should generate n nonoverlapping hotspots.[34] Thus the rising-edge slope of the readout electrical pulses can convey the number of photons,[29] adhering to the electrical rule that the rising time of generated voltage approximately follows the time constant $L_k/R_{hs}(n)$, where L_k represents the total kinetic inductance of the detector and the $R_{hs}(n)$ corresponds to the total resistance of all n hotspots. Although some modified readouts have been exploited to augment the PNR capability by using a wideband cryogenic amplifier[29] or by integrating an impedance-matching taper,[35] the PNR dynamic range still hovers around $3 - 4$, and the PNR fidelity is somewhat constrained in terms of readout distinguishability.

Recently, superconducting microstrip single-photon detectors (SMSPDs)[36–38] have shown saturated sensitivity to near-infrared single photons and have demonstrated over 90% system detection efficiency using low-energy-gap WSi[38] or ion-irradiated NbN.[37] SNSPDs and SMSPDs operate in a similar manner with respect to photon-number resolution. Their primary differentiation lies in the linewidth, granting SMSPDs several advantages, including improved signal-to-noise ratio (SNR) of response pulses, polarization insensitivity, and an increased active area. Here, we have presented, for the first time to our knowledge, compelling evidence of a large-dynamic-range and high-fidelity photon-number readout in an SMSPD. Even without the need for cryogenic amplifiers, a large-inductance SMSPD can resolve up to 10 photons, achieving a readout fidelity of 98% and 90% for four-photon and six-photon events, respectively. Furthermore, we demonstrated that the PNR capability of a conventional SNSPD or SMSPD can be enhanced by stretching the rising edges of photon-triggered electrical pulses, which encode the photon-number information.

By increasing the total inductance or strip width, the stretched rising edges become more distinguishable in terms of reading out the number of photon-induced hotspots and thus are more sensitive to photon numbers. For reading out the photon number in real time, we implemented a dual-channel timing setup to measure the rising-edge time. The combination of high fidelity, large dynamic range, and real-time measurement opens up possibilities for a variety of cutting-edge photon-number-resolving applications. For example, we illustrate the practicality of our system for quantum cryptography applications by creating a quantum random-number generator (QRNG) based on sampling the photon statistics of a coherent state. This method is fundamentally unbiased, robust to experimental imperfections and environmental noise, and invulnerable to eavesdropping.[9,39]

This article is structured into four parts: (1) first introducing the SMSPD's architecture and photon-number resolution, (2) then illustrating the influence mechanism of the photon-number readout capability, (3) next proposing the real-time readout setup, (4) and finally, applying the PNR system to a QRNG.

2 Results

2.1 Approaching True PNR with an SMSPD

The SMSPD comprises a single meandering microstrip. As shown in Fig. 1(a), the meandering microstrip is divided into three distinct functional segments for the purposes of detecting, connecting, and bending according to their width, which are designated as A, B, and C, respectively, and color-coded accordingly. The detecting section A features a circular active area of 50 μm diameter and contains a series of parallel 1-μm-wide microstrips with 100-nm gaps, resulting in a high fill factor of 91%. In the bending section C, we utilized the L-shaped layout for the microstrips to maintain a high fill rate while mitigating the current-crowding effect[38,40], which incorporates an optimized 90 deg turn before the 180 deg turnaround. The 90 deg turn transitions the strip width from 1.05 to 1.5 μm, while the 180 deg turnaround has a trip width of 1.5 μm and an interval of 2 μm. The connecting wires in part B for linking sections A and C are 1.05 μm wide and are spaced 50 nm apart from each other. This design, where strips for connecting and bending are wider than those for detection, aims for decreasing the impact of defects to increase the device yield and minimizing the current crowding to enhance the switching current. Figure 1(b) illustrates the simulated current density distribution in an L-shaped bend using the RF module of COMSOL Multiphysics. It is evident that the current density is highest in detecting section A, while in other sections, such as points b through e, it is lower. Particularly, the current density in point e in the bending section is only 87% of that in point a in the detection section. To ensure stable operation without a shunt resistor, the detector was connected in series with 1.2-μm-wide meandering microstrips, resulting in a total inductance of 6 μH. The detector was fabricated using a 7-nm-thick NbN film on a silica substrate and exhibited a switching current of 122 μA at the operation temperature of 2.2 K. Its basic performance (as shown in Figs. S1 and S2 in the Supplementary Material) is discussed in section 1 of Supplementary Material.

We investigated the multiphoton response of the SMSPD by using an attenuated 1064 nm pulsed laser. In contrast to a previously reported cryogenic readout,[29] we directly amplified the photon-triggered electrical pulses using a room-temperature low-noise amplifier (LNA1800) and captured them with
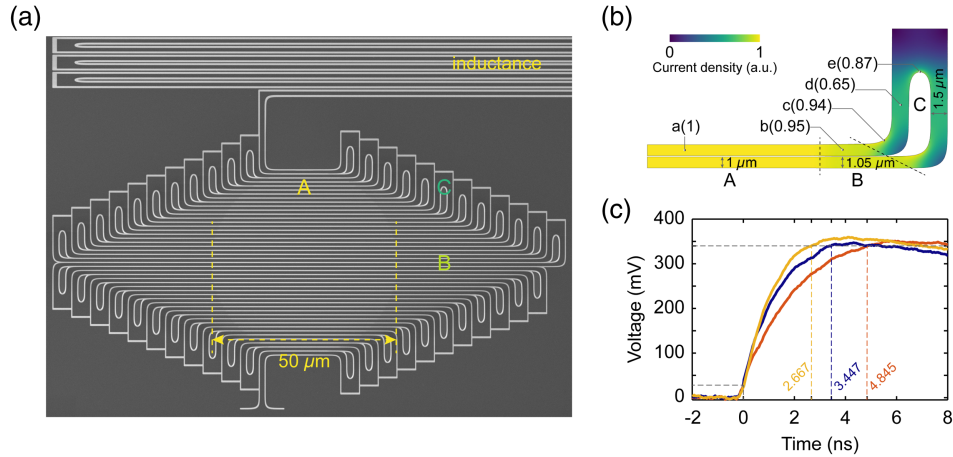
(a)

(b)

(c)

Fig. 1 SMSPD. (a) Scanning electron micrograph of the SMSPD. (b) Simulated current density distribution in three sections: detecting (A), connecting (B), and bending (C). Points a–e indicate the relative current density. This structure ensures a higher current density in the detecting section than in the other sections. (c) Rising section of typical output waveforms generated from different detections of one, two, and three photons.

a high-speed oscilloscope. In Fig. 1(c), the rising-edge section of typical output waveforms exhibited distinct slope separations. To determine the rising-edge time $\Delta\tau_{\text{rise}}$ of electrical pulses, we employed two fixed discrimination levels: a low level V_L set to the maximum value of the system's electrical noise, and a high level V_H set to the minimum amplitude of the electrical pulses, as shown in Fig. 1(c). Owing to the large inductance and relatively small resistance, the output pulses have a long time in rising edges. The corresponding rising-edge time of 4.845, 3.447, and 2.667 ns indicates one-, two-, and three-photon events, respectively. Figure 2(a) exhibits the histograms of the rising-edge time (black dots) at two effective mean photon numbers per pulse $\tilde{\mu}$ of 2.5 and 5.1. Here, $\tilde{\mu}$ took into account the detector efficiency and coupling losses. Notably, we observed distinct separations of rising-edge time for up to 10 photons. We group the counting probability for $n \geq 11$, as significant overlap renders these photon events indistinguishable.

In order to assign a photon number m for a detection event with pulse rising-edge time $\Delta\tau_{\text{rise}}$, a series of dividing thresholds $\tau_{k,1\leq k\leq 11}$ need to be determined. This allows us to assign the event to a photon number m, if $\tau_m < \Delta\tau_{\text{rise}} < \tau_{m+1}$. To begin, we fitted the histograms of rising-edge time with Gaussian models [color area in Fig. 2(a)]. Subsequently, we normalized each distribution $G_n(t)$ associated with the photon number n. The dividing thresholds were determined at the position of the intersection between two adjacent Gaussian distributions. Note that as the photon numbers increase, the center distance decreases, and the overlap between adjacent distributions increases—thus the certainty of assigning a photon number decays. To access the accuracy of the photon-number assignments using the rising-edge time of output pulses, we calculate the probability distribution of assigning photon number m to the detection event when n photons detected P_n^m, which is described as[41]

$$P_n^m = \int_{\tau_m}^{\tau_{m+1}} G_n(t)\mathrm{d}t. \tag{1}$$

Figure 2(b) illustrates the confusion matrix of photon-number assignment, providing insights into the readout fidelity of

n photons, represented by P_n^n. In the ideal case, the confusion matrix would be an identity matrix, with all diagonal terms equal to 1 and all nondiagonal terms equal to 0. Our readout quality approaches the ideal case in the low photon-number regime. For example, the readout fidelity achieves a parts-per-hundred-billion precision of $P_1^1 = 0.99999999993$ for photon number $n = 1$ and a parts-per-million precision of $P_2^2 = 0.999998$ for $n = 2$. For higher photon numbers, the readout fidelity gradually decreases. It remains above 0.98 for ≤ 4 photons but significantly decays to below 0.90 for ≥ 7 photons.

After establishing the dividing thresholds $\tau_{k,1\leq k\leq 11}$, the photon events in different threshold-to-threshold regions can be counted to reconstruct the photon statistics $Q(n)$. When the photon number ranges from 1 to 10, each hotspot has a length between 10 and 3 μm, estimated from electrothermal simulation. Since it is far smaller than the total length ($\sim$2000 μm) of the microstrip, the probability of hotspot overlap is negligible. Therefore, as shown in Fig. 2(c), the photon statistics $Q(n)$ directly followed the Poisson distribution $Q(n) = \tilde{\mu}^n e^{-\tilde{\mu}}/n!$ without requiring a conditional probability typically necessary for most array-based quasi-PNR detectors,[31] which indicates that the SMSPD infinitely approaches the true PNRD. The effective mean photon number per pulse $\tilde{\mu}$ is estimated by measuring the photon clicking probability $\eta_{\text{click}} = R_{\text{click}}/f_{\text{rep}}$ and solving the equation $1 - e^{-\tilde{\mu}} = \eta_{\text{click}}$, where R_{click} is the photon clicking rate and f_{rep} is the repetition rate of pulse laser.

2.2 Influence Mechanism of the Photon-Number Readout Capability

To investigate the influence mechanism of the PNR capability in SNSPDs/SMSPDs, we designed a comparison vector including five detectors with different widths and inductance: $100\,\text{nm} - 1\,\mu\text{H}$, $100\,\text{nm} - 3\,\mu\text{H}$, $100\,\text{nm} - 5\,\mu\text{H}$, $300\,\text{nm} - 5\,\mu\text{H}$, and $500\,\text{nm} - 5\,\mu\text{H}$. The SNSPDs with nanostrip widths of 100, 300, and 500 nm covered different circular active areas of 20, 30, and 50 μm diameter with a filling rate of 33%, 50%, and 50%. The target inductance was achieved by connecting in series with 1.5 times wider meandering nanostrips than the
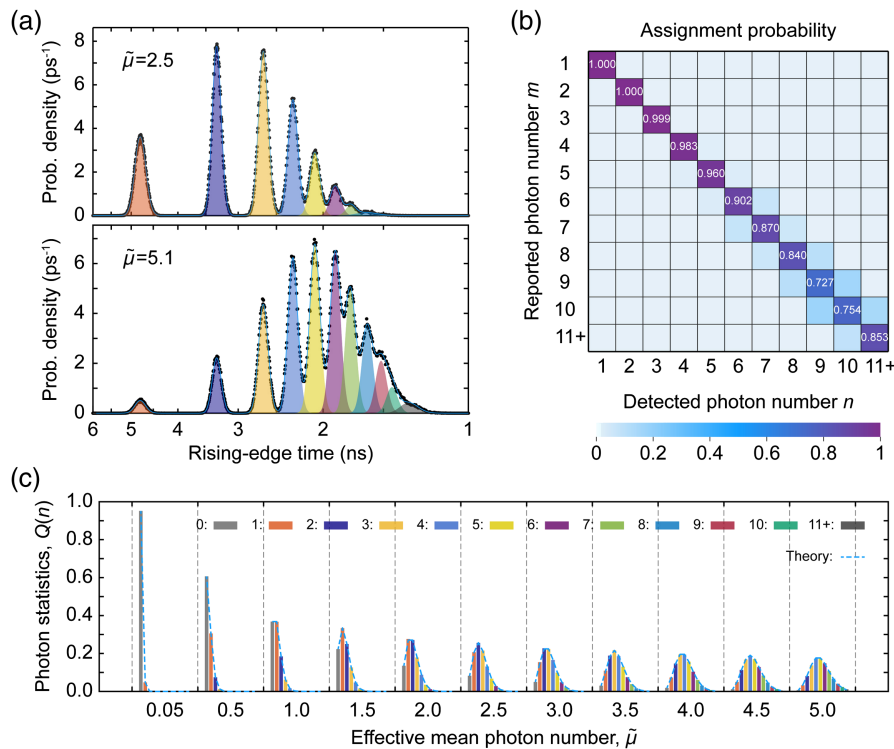
Fig. 2 Photon-number resolution in an SMSPD. (a) Histograms (dots) and Gaussian fitting (lines) of the rising-edge time of response pulses under pulsed laser illumination with an effective mean photon number $\tilde{\mu}$ at 2.5 and 5.1. Color areas represent the decomposed Gaussian functions. (b) Confusion matrix illustrating the probabilities of assigning n detected photons to m reported photons, where the diagonal terms P_n^n represent the photon-number readout fidelity. (c) Photon count statistics reconstructed from the distributions of pulse rising-edge time at different effective mean photon numbers $\tilde{\mu}$ ranging from 0.05 to 5. The measured photon count statistics (color bars) align closely with the Poisson statistics of the coherent source (dashed lines).

photon-sensitivity nanostrips. The nanostrips acting as inductance were located approximately 50 μm away from the photon-sensitivity area to avoid photon absorption.

Figures 3(a)–3(e) depict the histograms of rising-edge time of response pulses from the comparison vector. In general, detectors with larger inductance and wider strips exhibit improved photon-number resolution. Based on 100-nm wide strips [Figs. 3(a)–3(c)], the detector is only capable of distinguishing two photons. Traditional wisdom argues that a larger inductance imposes two disadvantages on SNSPDs, including degrading the SNR of rising edges and increasing the recovery time. However, the stretched rising edges are beneficial for photon-number discrimination due to more distinguished rising edges among different-photon-number events. As shown in Figs. 3(a)–3(c), by increasing the inductance, the overlaps between one- and two-photon events get smaller. Upon maintaining the inductance at 5 μH and increasing the strip width w, the PNR capability improves significantly. Therefore, the 100-nm wide detector can only achieve over 90% readout fidelity for assigning between single-photon and multiphoton events, while the 500-nm-wide and 1-μm-wide detectors can, respectively, resolve four and six photons with 90% readout fidelity. Note that in the subgraph of Fig. 3(a), the shoulder in the histogram of rising time exceeding 600 ps arises from the counting events at bends of meandering nanostrips, where the hotspot resistance is smaller than that of straight sections (as illustrated in Fig. S3

in the Supplementary Material). If ensuring full coupling of the incident photon onto the straight nanostrips, this phenomenon can also aid in eliminating intrinsic dark counts at the bends of meandering nanostrips.

We conclude that the phenomenon described above was caused by the limited bandwidth of the readout electronics and the SNR of response pulses. A universal amplifier for SNSPDs (such as LNA1800 here) typically has a 3 dB bandwidth of ∼1 GHz, which restricts the rise time (10%–90% amplitude) to τ_{lim} (∼300 ps). Consequently, when the intrinsic response pulses have a fast rising-edge time τ_{int} approaching or smaller than τ_{lim}, their rising edges will be broadened after passing through the amplifier, following $\sqrt{\tau_{\text{int}}^2 + \tau_{\text{lim}}^2}$. This addition of rising time prevents us from accurately acquiring the real rising time and also brings the pulse rising time of multiphoton events closer.

According to Eqs. (5) and (6), increasing the total inductance L_k of SNSPDs directly increases the intrinsic rising-edge time τ_{int} on the scale of $\sqrt{L_k}$, which subsequently weakens the bandwidth limit of readout electronics. We further fitted these histograms of rising-edge time with Gaussian models [color area in Figs. 3(a)–3(e)] to, respectively, extract the mean τ_{mu} and standard deviation τ_{std} of rising-edge time at each photon number n. By fitting these mean τ_{mu} versus photon number n with power functions, they scale approximatively as theoretical $n^{-0.5}$, except for the 100 nm − 1 μH detector, whose exponent is −0.39.
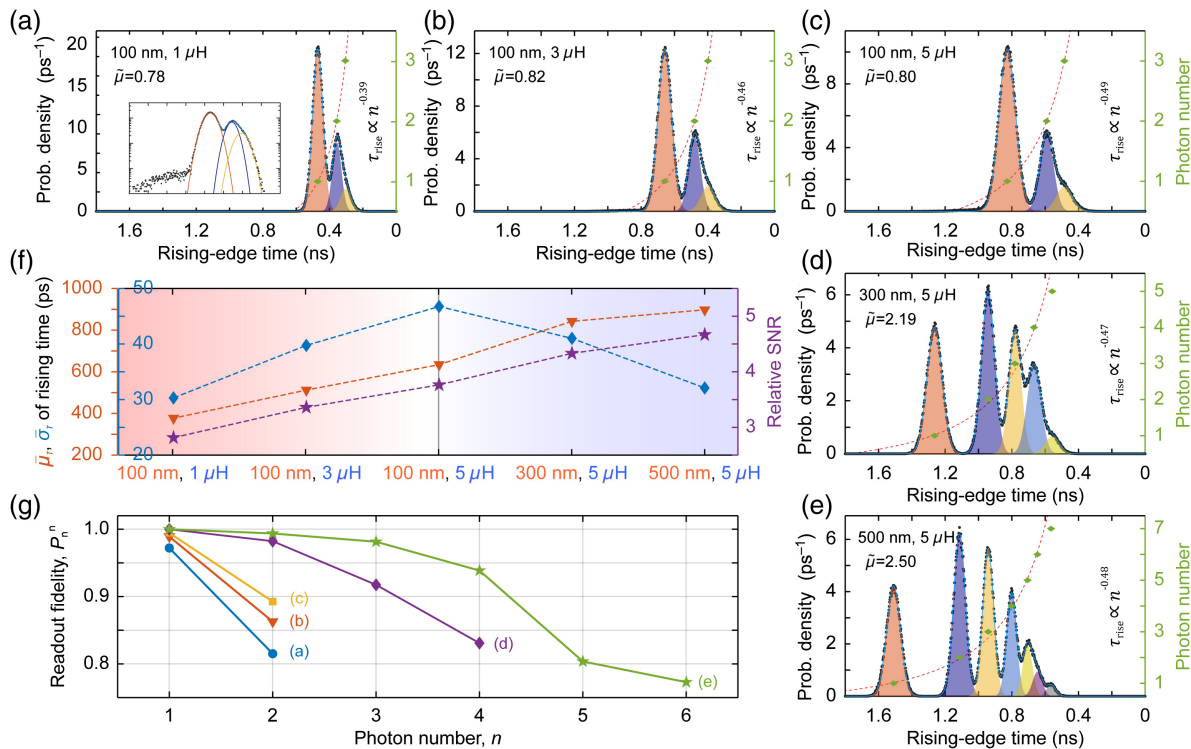
Fig. 3 Photon-number readout capability versus inductance and width. (a)–(e) Histograms and Gaussian fitting of the rising-edge time of response pulses generated from detectors with varying inductance and width. Black dots, measurement data; blue lines, Gaussian fitting results; color areas, decomposed Gaussian functions. The rising-edge time shows a power function with an exponent of 0.5 in relation to the photon number. Green diamonds, extracted mean of rising-edge time; orange dashed lines, fitted power functions. (f) The $\overline{\tau_m}$ and $\overline{\tau_{std}}$ of rising-edge time and relative SNR at different detector conditions. (g) Photon-number readout fidelity of detectors with different inductance and width, which are extracted from (a)–(e).

These fitting results further support the above analysis, indicating that readout bandwidth weakens the photon-number readout capability. Increasing the width leads to a smaller hotspot resistance and hence a longer rising-edge time τ_{int} of response pulses, which similarly scale approximately as $\sqrt{w}$. Additionally, a wider superconducting strip increases the bias current linearly and improves the SNR, and reduces the jitter of rising-edge time. Figure 3(f) presents the average τ_{mu} and τ_{std} (referred to as $\overline{\tau_{mu}}$ and $\overline{\tau_{std}}$) of different superconducting strip detectors. We also define the relative SNR as $2(\tau_{mu,i+1} - \tau_{mu,i})/(\tau_{std,i+1} + \tau_{std,i})$ to evaluate the quantitative impact on photon-number readout capability. When the strip width is fixed at 100 nm and inductance increases, although the $\overline{\tau_{mu}}$ and $\overline{\tau_{std}}$ both increase, the relative SNR still becomes larger, which implies a better readout fidelity [Fig. 3(g)]. Increasing the strip width increases the $\overline{\tau_{mu}}$ but reduces $\overline{\tau_{std}}$, as a result of which the relative SNR was significantly enhanced. In summary, larger inductances and wider strips can enhance the photon-number readout capability by stretching the rising edges to break the bandwidth limitation of readout electronics and by enhancing the SNR of readout pulses to reduce the rising-time jitter.

2.3 Real-time Readout Setup

For many PNR applications, it is crucial to utilize the photon-number information as immediate feedback.[4–6,10,11,42] However,

the traditional approach of waveform discrimination using a digitizer necessitates considerable data acquisition on the order of 1 GB/s, coupled with extensive postprocessing, thereby impeding real-time access to photon-number information. Benefiting from the projection mechanism from photon number to rising-edge time, we can reduce the data stream to the order of 1 MB/s and thus enable real-time readout by using a dual-channel constant-threshold timing tagger. As illustrated in Fig. 4(a), the response signal after the low-noise amplifier is divided into two equal pulses by a power splitter. Then the pair of pulses is measured by two time-to-digital converters (TDCs) at two different voltage thresholds. One TDC measures the time stamp t_L at the low discrimination level V_L, while the other one obtains the high-level (V_H) time stamp t_H. Compared to time-correlated jitter measurement,[6] our method is not affected by intrinsic timing jitter, although it does reduce the SNR of pulses. More importantly, the photon arrival time represented as $(t_L + t_H)/2$ here does not participate in discriminating the photon number, which is necessary in PNR-enhanced communication[10] and lidar.[11]

To validate the accuracy of the dual-channel TDCs method, we compared the histograms of time difference $t_H - t_L$ generated from this setup with that obtained directly from an oscilloscope without a splitter. As shown in Fig. 4(b), the 2-TDC method can distinguish up to ten photons, which was basically consistent with the results of the oscilloscope method. However,
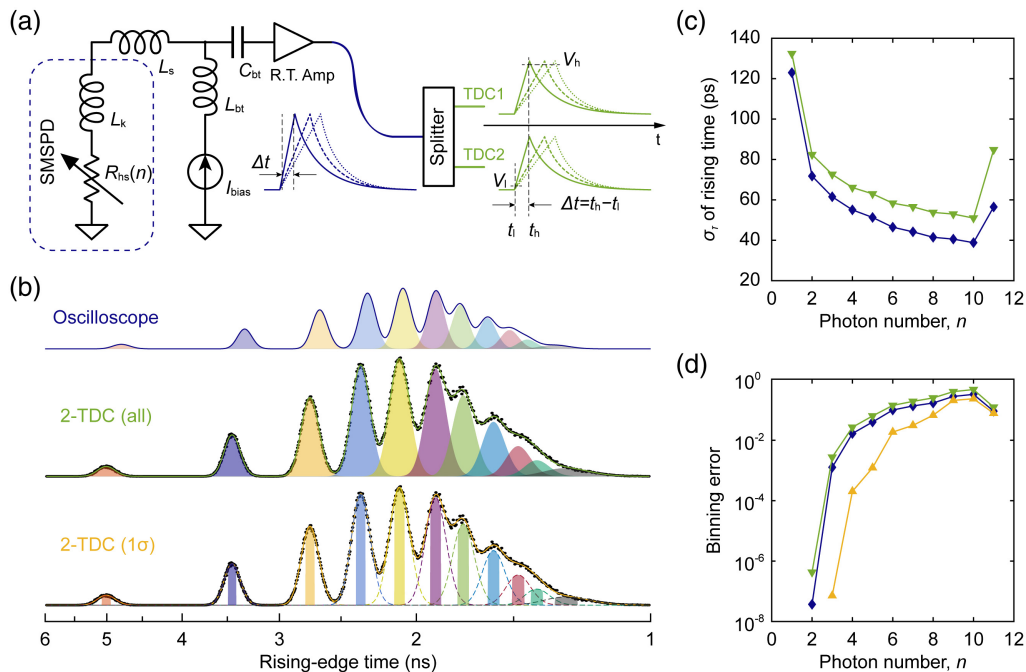
Fig. 4 Real-time readout and binning error reduction. (a) Equivalent circuit diagram of the setup. The response pulse through the power splitter is divided into two equal pulses, which then enter two TDCs. One TDC measures the high-level (V_H) time stamp t_H, while the other TDC measures the low-level (V_L) time stamp t_L. (b) Histograms and Gaussian fitting of the rising-edge time of response pulses measured by an oscilloscope without a splitter or the 2-TDC setup (all data and 1σ data). (c) The σ_τ of rising-edge time for two readout setups. The results using the 2-TDC setup are slightly inferior to those obtained using an oscilloscope, which is due to the additional timing jitter of the TDCs. (d) The photon-number binning error for three readout methods including oscilloscope, 2-TDC (all data), and 2-TDC (1σ data).

the readout fidelity P_n^n of the 2-TDC method is always lower than that of the oscilloscope method [Fig. 4(c)]. The slight decrease in PNR capability results from the increased jitter of rising-edge time [Fig. 4(c)], which is attributed to two factors: the decreased SNR of electrical pulses and the additional timing jitter σ_{TDC} of the TDCs. We first evaluated the SNR of pulses before and after the power splitter. Before the splitter, the standard deviation σ_{th} of thermal noise, the standard deviation σ_{amp}, and the mean V_{amp} of pulse amplitudes were 1.9, 3.75, and 354.6 mV, while after the splitter, these values were 1.9, 2.71, and 246.2 mV. The thermal noise remained constant, but amplitude noise (including thermal noise and amplitude fluctuation) decreased with amplitude; thus the pulse SNR V_{amp}/σ_{amp} only decayed a little, from 94.56 to 90.85. This observation indicates that splitting the electronic pulses does not significantly compromise the SNR. In addition to the decreased SNR of readout pulses, the TDC's timing jitter is the primary cause of the weakened PNR capability. The TDC in our experiment has an RMS timing jitter σ_{TDC} of 34 ps, which increased the measurement uncertainty of rising-edge time by $\sqrt{\sigma_\tau^2 + \sigma_{TDC}^2}$. Therefore, the 2-TDC setup is an effective readout method that minimally affects the SNR but only requires low-jitter TDCs.

If a partial relinquishment of counts is deemed acceptable, the accuracy of assigning photon numbers can be significantly improved by re-establishing the dividing regions near the centers of each decomposed Gaussian function. Only events falling within this region are included in the statistics [see Fig. 4(b)]. If the regions of certainty are confined within $\pm\frac{1}{2}\sigma_\tau$ of each peak, approximately 62% of data is discarded. However, this results in a decrease in the binning error rates from 24% to 6% or lower for the first eight photon numbers, as depicted in Figs. 4(b) and 4(d). In summary, this postselection can reduce the binning error rates by $<1/4$ but at the cost of a 62% loss in detection efficiency.

2.4 Unbiased Quantum Random-Number Generation

Due to the significant improvement in the dynamic range and readout speed of the SMSPD-based PNRD, they can now be directly employed in QRNGs. Random numbers play a critical role in science and technology, with applications ranging from simulation to cryptography. QRNGs leverage the inherent randomness in quantum mechanics to generate perfect sources of entropy for random numbers.[43] Classical or quantum light serves as a convenient and affordable source of quantum randomness. QRNGs based on homodyne measurement of random vacuum fluctuations can easily achieve high bit rates up to Gbit/s,[44,45] but these methods also suffer from nonuniform randomness with bias. Photon-counting methods that harness the intrinsic randomness of photon-number statistics are inherently unbiased.[39,42,43] However, the main challenges lie in achieving high PNR capability and detector speed. In this work, we have successfully implemented a QRNG by sampling the parity of

the Poisson distribution of a coherent state using an SMSPD. This approach is resilient against various experimental imperfections (such as photon loss, detector inefficiency, phase and amplitude fluctuations of the laser), environmental noise contamination, and potential eavesdropping.[9,39]

To generate random numbers, we simply transform photon-number detections into binary outputs using the $\pm\frac{1}{2}\sigma_n$ method, as depicted in Fig. 5(a). In this conversion, odd photon-number events are assigned an outcome of "1," while even ones are assigned "0." According to Gerry's theory,[39] the expectation of parity is given as

$$\langle\hat{\Pi}\rangle = e^{-2\tilde{\mu}}, \qquad (2)$$

where $\tilde{\mu}$ represents the mean photon number of the coherent state. Consequently, the inherent bias diminishes exponentially as the intensity of the coherent state increases. For instance, when $\tilde{\mu} = 5.1$, the theoretical expectation is $e^{-10.2} \approx 3.7 \times 10^{-5}$. We subjected the 10^9 random bits generated by our protocol to a battery of tests from the NIST suite of randomness tests.[46] The extensive experimental data were divided into 1000 separate smaller streams of 10^6 bits each. With a significance level of $\alpha = 0.01$, all proportions passing a particular test lie within the confidence interval of 0.98 to 1, as shown in Fig. 5(b). These results validate the randomness of our measurements across all considered tests. However, due to finite sampling and binning errors, the measured parity in our experiment

only reached 9.7×10^{-4}, which leads to the "frequency" test reaching the upper bound of 1. In the future, by leveraging a low-noise cryogenic readout to enhance the SNR of readout pulses, we can increase photon-number resolution and decrease the binning error rate, thus reducing the residual bias. In our experiment, the pulsed laser was operated at a repetition rate of 500 kHz to ensure full recovery of the SMSPD. Although slower than a conventional SNSPD, this rate is still 1 to 2 orders of magnitude faster than a TES.[14] In the future, by connecting a resistor in series, the counting rate can be increased to tens of megahertz.[47,48]

3 Conclusion

We have first demonstrated that a large-inductance SMSPD is capable of resolving photon numbers up to 10, concurrently achieving high readout fidelity of over 98% and 90% for photon numbers up to 4 and 6, respectively. This is primarily attributed to the positive influence of large kinetic inductance and wide microstrips on the rising-edge time of readout pulses, enabling enhanced photon-number resolution. By incorporating the proposed 2-TDC method, we have further achieved real-time photon-number readout, which outperforms traditional data acquisition methods by 3 orders of magnitude in terms of efficiency. Compared to other SNSPD-based PNR techniques, our solution stands out for its high fidelity, large dynamic range, and real-time characterization. Additionally, it boasts a simplified device structure, ease of fabrication, and streamlined
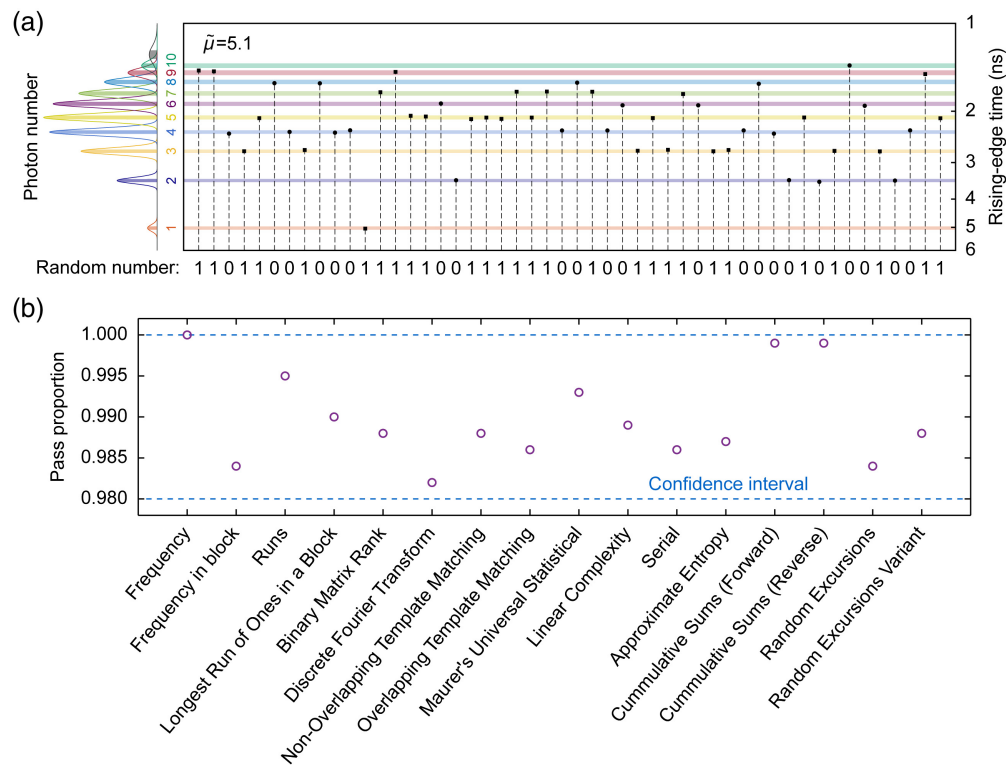

Fig. 5 Generation and testing of quantum random numbers. (a) Operating principle of the QRNG. The graph on the right shows a sequence consisting of 50 rising-edge times, along with the random numbers at an effective mean photon number per pulse $\tilde{\mu}$ of 5.1. (b) Results of the NIST randomness tests on 1000×10^6 binary bit strings. The confidence interval, represented by the dashed blue lines, ranges from 0.98 to 1. It is calculated using a normal distribution as an approximation to the binomial distribution.

readout processes. Moreover, we have demonstrated the utility of our PNR system in creating an unbiased and robust QRNG by sampling the photon-number statistics of a coherent state. Beyond QRNG, as the detection efficiency of SMSPDs continues to increase,[49] we envision its broad applicability in a variety of cutting-edge technologies, such as photonic quantum computing,[50] Boson sampling,[51] and quantum metrology.[52]

4 Appendix: Materials and Methods

4.1 Fabrication

Here, 7-nm-thick NbN film was deposited on a silicon substrate with a 268-nm-thick thermal oxide layer using reactive DC magnetron sputtering. The NbN film had a critical temperature of $T_c = 7.6$ K. Then, the NbN film was patterned into a meandered nanowire structure using 100 kV electron-beam lithography with a 70-nm-thick positive-tone resist (ZEP520A) and reactively etched in CF_4 plasma at a pressure of 4 Pa and RF power of 50 W.

4.2 Numerical Calculation

To analyze the effects of inductance and width on rising-edge time, we utilize the electrothermal feedback model. The lumped equivalent electrical model of the SNSPD consists of a hotspot-number-dependent resistor in series with a kinetic inductor. After the initiation of a detection event, the dynamics of the 1D electrothermal system are governed by the interaction between the SNSPD and the readout circuit, which can be mathematically described as[53]

$$\frac{dR_{hs}}{dt} = 2\frac{R_{sq}}{w}v_{NS},\tag{3}$$

$$L_k\frac{dI_d}{dt} + nR_{hs}I_d = (I_b - I_d)R_L,\tag{4}$$

where R_{hs} represents the resistance of individual hotspots, R_{sq} is the sheet resistance of superconducting film in the normal state, w denotes the strip's width, I_b and I_d are the bias current and current through the SNSPD, respectively, and R_L represents the load impedance of the readout circuit. The normal-superconducting boundary propagates at a velocity of v_{NS}. Although this expansion rate v_{NS} is dependent on time,[54] here we treat it to a constant value to make Eqs. (3) and (4) easier to solve. Its multiplication with the resistance of unit length R_{sq}/w quantifies the growing rate of resistance.[53] By solving the above coupled Eqs. (3) and (4), we can approximately estimate the maximum value of total hotspot resistance and the corresponding rising-edge time:

$$R_{hs}(n) = nR_{hs,max} \propto \sqrt{\frac{L_k R_{sq} v_{NS} n}{w}},\tag{5}$$

$$\tau_{rise}(n) \approx \frac{L_k}{R_{hs}(n)} \propto \sqrt{\frac{L_k w}{R_{sq} v_{NS} n}}.\tag{6}$$

In Sec. 2 of the Supplementary Material, more accurate results are obtained through a finite-element simulation of the electrothermal process.[55–57]

Disclosures

The authors declare no competing financial interests.

Code and Data Availability

The data that support the findings of this study are available from the corresponding author upon request.

Author Contributions

L.-D.K. conceived the idea and designed the experiment. T.-Z.Z., L.-D.K., and X.-Y.L. fabricated the device. L.-D.K. and T.-Z.Z. performed the measurements. All the authors discussed the results. L.-D.K. and L.-X.Y. wrote the manuscript with input from all authors.

References

1. H.-S. Zhong et al., "Quantum computational advantage using photons," *Science* **370**, 1460–1463 (2020).
2. L. S. Madsen et al., "Quantum computational advantage with a programmable photonic processor," *Nature* **606**, 75–81 (2022).
3. Y.-A. Chen et al., "An integrated space-to-ground quantum communication network over 4,600 kilometres," *Nature* **589**, 214–219 (2021).
4. E. Knill, R. Laflamme, and G. J. Milburn, "A scheme for efficient quantum computation with linear optics," *Nature* **409**, 46–52 (2001).
5. J. L. O'Brien, "Optical quantum computing," *Science* **318**, 1567–1570 (2007).
6. S. I. Davis et al., "Improved heralded single-photon source with a photon-number-resolving superconducting nanowire detector," *Phys. Rev. Appl.* **18**, 064007 (2022).
7. J. Hloušek et al., "Accurate detection of arbitrary photon statistics," *Phys. Rev. Lett.* **123**, 153604 (2019).
8. E. Waks et al., "Direct observation of nonclassical photon statistics in parametric down-conversion," *Phys. Rev. Lett.* **92**, 113602 (2004).
9. M. Eaton et al., "Resolution of 100 photons and quantum generation of unbiased random numbers," *Nat. Photonics* **17**, 106–111 (2022).
10. F. E. Becerra, J. Fan, and A. Migdall, "Photon number resolution enables quantum receiver for realistic coherent optical communications," *Nat. Photonics* **9**, 48–53 (2015).
11. L. Cohen et al., "Thresholded quantum LiDAR: exploiting photon-number-resolving detection," *Phys. Rev. Lett.* **123**, 203601 (2019).
12. M. Jönsson and G. Björk, "Evaluating the performance of photon-number-resolving detectors," *Phys. Rev. A* **99**, 043822 (2019).
13. R. H. Hadfield, "Single-photon detectors for optical quantum information applications," *Nat. Photonics* **3**, 696–705 (2009).
14. A. E. Lita et al., "Development of superconducting single-photon and photon-number resolving detectors for quantum applications," *J. Lightwave Technol.* **40**, 7578–7597 (2022).
15. E. Waks et al., "High-efficiency photon-number detection for quantum information processing," *IEEE J. Sel. Top. Quantum Electron.* **9**, 1502–1511 (2003).

16. E. J. Gansen et al., "Photon-number-discriminating detection using a quantum-dot, optically gated, field-effect transistor," *Nat. Photonics* **6**, 585–588 (2007).
17. B. E. Kardynał, Z. L. Yuan, and A. J. Shields, "An avalanche-photodiode-based photon-number-resolving detector," *Nat. Photonics* **2**, 425–428 (2008).
18. L. A. Jiang, E. A. Dauler, and J. T. Chang, "Photon-number-resolving detector with10 bits of resolution," *Phys. Rev. A* **75**, 062325 (2007).
19. I. E. Zadeh et al., "Superconducting nanowire single-photon detectors: a perspective on evolution, state-of-the-art, future developments, and applications," *Appl. Phys. Lett.* **118**, 190502 (2021).
20. P. Hu et al., "Detecting single infrared photons toward optimal system detection efficiency," *Opt. Express* **28**, 36884–36891 (2020).
21. D. V. Reddy et al., "Superconducting nanowire single-photon detectors with 98% system detection efficiency at 1550 nm," *Optica* **7**, 1649–1653 (2020).
22. J. Chang et al., "Detecting telecom single photons with 99.5−2.07+0.5% system detection efficiency and high time resolution," *APL Photonics* **6**, 036114 (2021).
23. A. S. Mueller et al., "Free-space coupled superconducting nanowire single-photon detector with low dark counts," *Optica* **8**, 1586–1587 (2021).
24. W. J. Zhang et al., "Fiber-coupled superconducting nanowire single-photon detectors integrated with a bandpass filter on the fiber end-face," *Supercond. Sci. Technol.* **31**, 035012 (2018).
25. I. Craiciu et al., "High-speed detection of 1550 nm single photons with superconducting nanowire detectors," *Optica* **10**, 183–190 (2023).
26. G. V. Resta et al., "Gigahertz detection rates and dynamic photon-number resolution with superconducting nanowire arrays," *Nano Lett.* **23**(13), 6018–6026 (2023).
27. B. Korzh et al., "Demonstration of sub-3 ps temporal resolution with a superconducting nanowire single-photon detector," *Nat. Photonics* **14**, 250–255 (2020).
28. L. You, "Superconducting nanowire single-photon detectors for quantum information," *Nanophotonics* **9**, 2673 (2020).
29. C. Cahall et al., "Multi-photon detection using a conventional superconducting nanowire single-photon detector," *Optica* **4**, 1534–1535 (2017).
30. L. Kong et al., "Probabilistic energy-to-amplitude mapping in a tapered superconducting nanowire single-photon detector," *Nano Lett.* **22**, 1587–1594 (2022).
31. A. Divochiy et al., "Superconducting nanowire photon-number-resolving detector at telecommunication wavelengths," *Nat. Photonics* **2**, 302–306 (2008).
32. S. Jahanmirinejad et al., "Photon-number resolving detector based on a series array of superconducting nanowires," *Appl. Phys. Lett.* **101**, 072602 (2012).
33. R. Cheng et al., "A 100-pixel photon-number-resolving detector unveiling photon statistics," *Nat. Photonics* **17**, 112–119 (2022).
34. K. L. Nicolich et al., "Universal model for the turn-on dynamics of superconducting nanowire single-photon detectors," *Phys. Rev. Appl.* **12**, 034020 (2019).
35. D. Zhu et al., "Resolving photon numbers using a superconducting nanowire with impedance-matching taper," *Nano Lett.* **20**, 3858–3863 (2020).
36. I. Charaev et al., "Large-area microwire MoSi single-photon detectors at 1550 nm wavelength," *Appl. Phys. Lett.* **116**, 242603 (2020).
37. G.-Z. Xu et al., "Superconducting microstrip single-photon detector with system detection efficiency over 90% at 1550 nm," *Photonics Res.* **9**, 958–967 (2021).
38. D. V. Reddy et al., "Broadband polarization insensitivity and high detection efficiency in high-fill-factor superconducting microwire single-photon detectors," *APL Photonics* **7**, 051302 (2022).
39. C. C. Gerry et al., "Proposal for a quantum random number generator using coherent light and a non-classical observable," *J. Opt. Soc. Am. B* **39**, 1068–1074 (2022).
40. M. Jönsson et al., "Current crowding in nanoscale superconductors within the Ginzburg-Landau model," *Phys. Rev. Appl.* **17**, 064046 (2022).
41. L. Assis Morais et al., "Precisely determining photon-number in real time," arXiv:2012.10158 (2020).
42. M. Ren et al., "Quantum random-number generator based on a photon-number-resolving detector," *Phys. Rev. A* **83**, 023820 (2011).
43. M. Herrero-Collantes and J. C. Garcia-Escartin, "Quantum random number generators," *Rev. Mod. Phys.* **89**, 015004 (2017).
44. C. Gabriel et al., "A generator for unique quantum random numbers based on vacuum states," *Nat. Photonics* **4**, 711–715 (2010).
45. B. Bai et al., "18.8 Gbps real-time quantum random number generator with a photonic integrated chip," *Appl. Phys. Lett.* **118**, 264001 (2021).
46. B. Lawrence et al., Special publication (NIST SP), National Institute of Standards and Technology, Gaithersburg, Maryland (2010).
47. J. K. W. Yang et al., "Modeling the electrical and thermal response of superconducting nanowire single-photon detectors," *IEEE Trans. Appl. Supercond.* **17**, 581–585 (2007).
48. C. L. Lv et al., "Large active area superconducting single-nanowire photon detector with a 100 μm diameter," *Supercond. Sci. Technol.* **30**, 115018 (2017).
49. P. Zolotov et al., "High-resistivity niobium nitride films for saturated-efficiency SMSPDs at telecom wavelengths and beyond," *Appl. Phys. Lett.* **122**, 152602 (2023).
50. P. Kok et al., "Linear optical quantum computing with photonic qubits," *Rev. Mod. Phys.* **79**, 135–174 (2007).
51. Y.-H. Deng et al., "Gaussian Boson sampling with pseudo-photon-number-resolving detectors and quantum computational advantage," *Phys. Rev. Lett.* **131**, 150601 (2023).
52. J. C. F. Matthews et al., "Towards practical quantum metrology with photon counting," *NPJ Quantum Inf.* **2**, 16023 (2016).
53. A. J. Kerman et al., "Electrothermal feedback in superconducting nanowire single-photon detectors," *Phys. Rev. B* **79**, 100509 (2009).
54. M. Ejrnaes et al., "Time-resolved observation of fast hotspot dynamics in superconducting nanowires," *Phys. Rev. B* **81**, 132503 (2010).
55. A. D. Semenov et al., "Analysis of the nonequilibrium photoresponse of superconducting films to pulsed radiation by use of a two-temperature model," *Phys. Rev. B* **52**, 581–590 (1995).
56. M. Sidorova et al., "Phonon heat capacity and self-heating normal domains in NbTiN nanostrips," *Supercond. Sci. Technol.* **35**, 105005 (2022).
57. A. Dane et al., "Self-heating hotspots in superconducting nanowires cooled by phonon black-body radiation," *Nat. Commun.* **13**, 5429 (2022).

Ling-Dong Kong received his PhD from Nanjing University, Nanjing, China, in 2022. He is currently a postdoctoral researcher with SIMIT, CAS, Shanghai, China. His research interests include superconducting electronics, and single-photon detection, imaging, and spectroscopy.

Tian-Zhu Zhang is a doctoral candidate student at SIMIT, CAS. Currently, he is working on superconducting nanowire single-photon detectors.

Xiao-Yu Liu received his MS degree from Nanjing University, Nanjing, China, in 2011. Since 2011, he has joined SIMIT, CAS, Shanghai, China. He is mainly engaged in the research of micro/nanoprocessing technology.

Hao Li received his BS degree in optical information science and technology from Jilin University, Changchun, China, in 2008, and his PhD in microelectronics and solid-state electronics from SIMIT, CAS, Shanghai, China, in 2013. In 2020, he was promoted to be a research professor with the SNSPD Group. His current research interests include optimal single-photon detection, multispectral/broadband single-photon detectors, and integration and applications of SNSPDs.

Zhen Wang received his PhD in electrical engineering degree from the Nagaoka University of Technology, Nagaoka, Japan, in 1991. From 1991 to 2013, he was with the National Institute of Information and Communications Technology (NICT), Japan. He was a fellow of NICT. He is currently a research professor with the SIMIT, CAS, Shanghai, China. His research interests include superconducting electronics, including superconducting devices and physics, superconducting SIS terahertz mixers, and photon detectors.

Xiao-Ming Xie received his BS degree from Wuhan University in 1985. From 1985 to 1990, he received his MSc and PhD degrees, respectively, in SIMIT, CAS. From 1993 to 1995, he worked as a visiting professor at Ecole Supérieure de Physique et de Chimie Industry (ESPIC) in Paris. He is currently the director of SIMIT, CAS. His research interest covers basic research on superconductivity, graphene quantum materials, and superconducting quantum interference device (SQUID).

Li-Xing You received his BS, MS, and PhD degrees in physics from Nanjing University, in 1997, 2001, and 2003, respectively. He was a postdoctoral researcher at Chalmers University of Technology and University of Twente from 2003 to 2006. In 2006, he was a guest researcher at the NIST, Boulder, CO, USA. Since 2007, he has been a research professor with SIMIT, CAS, Shanghai, China. His research interests include superconductive electronics, micro/nanosuperconductive devices, and high-frequency applications.